AKARI, a Light to Illuminate the Misty Universe
ASP Conference Series, Vol. 418, © 2009
T. Onaka, G. J. White, T. Nakagawa, and I. Yamamura

Observations of Interstellar and Circumstellar Ice

Yuri Aikawa,[1] Jennifer A. Noble,[2] Itsuki Sakon,[3] Dai Kamuro,[1]
Naoki Irimichi,[1] Klaus M. Pontoppidan,[4] Helen Fraser,[2]
Motohide Tamura,[5] Hiroshi Terada,[5] Munetaka Ueno,[6] and
AFSAS team

[1]*Department of Earth and Planetary Sciences, Kobe University, Japan*
[2]*Department of Physics, University of Strathclyde, UK*
[3]*Department of Astronomy, University of Tokyo, Japan*
[4]*California Institute of Technology, USA*
[5]*National Astronomical Observatory of Japan, Japan*
[6]*Institute of Space and Astronautical Science, JAXA, Japan*

Abstract. We observed ice absorption bands at NIR (2.5μm-5.0μm) towards field stars behind molecular clouds and low-mass YSOs with edge-on disk. We developed and tested a procedure to reduce the slitless spectroscopy data of extended object and the data with multiple objects in one field of view. Absorption bands of H_2O, CO_2 and CO are clearly detected towards field stars and YSOs. The spectral type and visual extinction of each field star are estimated using color-color diagram. The visual extinction of our field stars ranges from 15 mag to 25 mag. The column density of H_2O ice towards our target stars ranges from 3×10^{17}cm^{-2} to 1×10^{19} cm^{-2}, while the CO_2 ice column density is $(1-7)\times10^{17}$ cm^{-2}. These ice column densities are found to be roughly proportional to visual extinction.

1. Introduction

In molecular clouds, chemical reactions proceed both in the gas-phase and on grain-surfaces. The gaseous molecule collides and are adsorbed onto grain-surface to form ice mantle, and ice is desorbed to the gas-phase upon heating. In the gas-phase, two molecules or atoms collide to mainly produce two products (AB+C $\rightarrow$ A+BC), so that the excess energy is discarded as the kinetic energy of the products. On the grain-surfaces, on the other hand, two atoms or molecules can be associated by depositing the excess energy onto the grain surface. Hence, the grain surface is an important formation site of molecules which cannot efficiently be formed in the gas-phase, such as H_2O and CH_3OH. Adsorption of molecules and subsequent gain-surface reactions make the grain surface an important reservoir of elements. For example, about 10 % of elemental abundance of oxygen exists as water ice in molecular clouds (Wittet 1993); gas-phase C/O ratio is significantly affected by oxygen depletion onto grains.

The grain-surface reactions are, however, difficult to model or predict. While significant efforts and progresses have been made in theoretical modeling and laboratory experiments (Stantcheva et al. 2002; Watanabe & Kouchi 2002), it is important to observe ice in various physical conditions to understand the composition and formation processes of interstellar ice.

Ice in molecular clouds is observed as absorption bands towards background stars or embedded stars. Ground-based telescopes have long been observing H_2O ice and CO ice (Wittet 1993). But they are restricted to "atmospheric window"; CO_2 band at 4.27 μm and the shorter wavelength wing of 3.05 μm H_2O band cannot be observed from the ground. *Infrared Space Observatory (ISO)* was the first to observe full wavelength region from 2μm to 20 μm, and also the first to clearly detect CO_2 ice (Gibb et al. 2004). Although *ISO* was very successful, it mainly targeted towards high-mass YSOs, because sensitivity was not high enough to observe low-mass YSOs and faint field stars. Recently *Spitzer Space Telescope (SST)* performed spectroscopic observation at mid-infrared towards field stars and low-mass YSOs. Highlights of ice observation by *SST* includes extensive studies on CO_2 band at 14 μm (e.g. Whittet et al. 2007; Pontoppodan et al. 2008) and detection of CH_4 ice(Öberg et al. 2008). *AKARI*, on the other hand, has spectroscopic mode at NIR with high enough sensitivity to observe field stars and low-mass YSOs.

Another strong point of *AKARI* is its slitless spectroscopy mode. In astrochemical studies, spatial distribution of molecules gives us an important clue on chemical processes. For example, comparison of the emission map of dust continuum and gas-phase molecular lines in prestellar cores revealed a phenomenon called "chemical fractionation": CO is depleted at the core center, while N-bearing species are not. It indicates that CO is so abundant that its depletion onto grains significantly changes the gas-phase reaction network (e.g. Aikawa et al. 2005). Unlike emission lines, ice absorption bands tell us the ice column densities along a line of sight towards a light source. In order to derive spatial distribution of ice in molecular clouds, we have to observe many field stars (Murakawa et al. 2000; Pontoppidan et al. 2006). Such ice mapping is a suitable project for slitless spectroscopy mode of *AKARI*.

The rest of this paper is organized as follows. Observational settings are described in §2. We describe how we extract spectrum from slitless spectroscopy data, determine the continuum, and calculate the ice column densities in §3. The derived ice column densities towards background stars and YSOs are presented in §4.

2. Observation

Our ice observations were performed as two open-time projects: *ISICE* (P.I. Y. Aikawa) and *IMAPE* (P.I. H. J. Fraser). In *ISICE* we observed 25 FOV towards well known molecular cloud cores and 7 low-mass YSO with edge-on disks with grism mode. In *IMAPE*, we used both grism and prism mode to observe cores from *Spitzer* "c2d" targets. In this paper we present NIR results from *ISICE*, while Noble et al. (in this volume) report results from *IMAPE* project. Spectral resolution is ~ 100 for grism mode and ~ 20 for prism mode.

To illustrate how our data look like, Figure 1 shows reference images and dispersed images towards molecular cloud LM226 and class 0 object with edge-on disk L1527. The center of the LM226 is set at the center of 1'$\times$ 1' window.

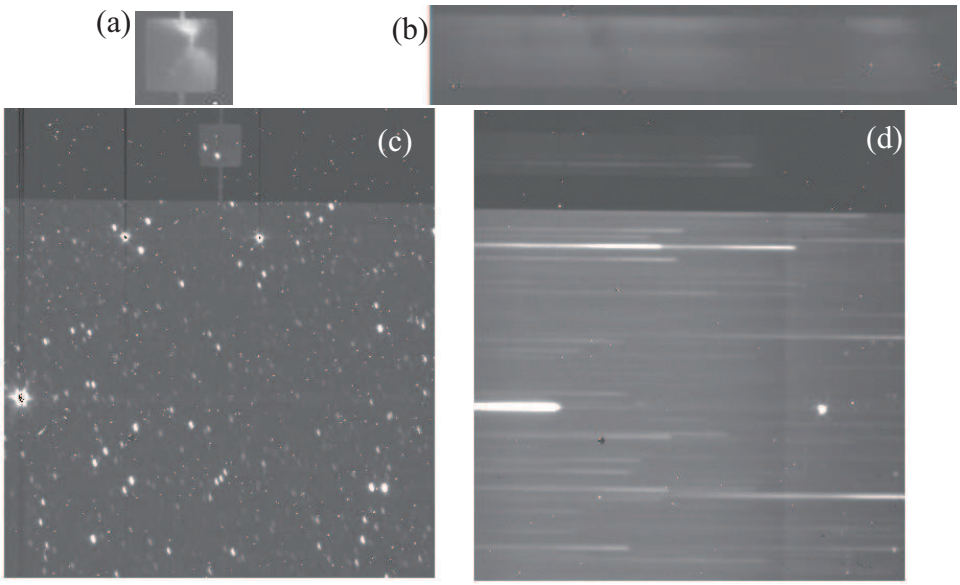

Figure 1. Reference image and spectrum image of L1527 (a)(b) and LM226 (c)(d).

3. Data Reduction and Analysis

3.1. Reduction of the Spectrum Image

The reduction pipeline provided by the *AKARI* project team did not work well for our targets. The pipeline automatically defines the area surrounding point sources as "sky." Since we have several tens of field stars in our FOV, "sky" defined as such often contains another source. Some spectra partially overlap with each other, which cannot be disentangled by the pipeline.

In order to derive spectrum from the data, we developed our own programs referring to the reduction method by Sakon et al. (2009). Firstly, we remove cosmic-ray from the dark and subtract it from the N3 and NG images. We shift and add NG frames after removing the cosmic-ray. The local sky is hand-selected, avoiding objects and bad pixels. In the case of the extended object, such as L1527, we selected from the archive the 1' × 1' spectrum image which can be used as sky; the data should be taken at similar period and coordinate to our target and should be almost dark. After the sky subtraction, we define the spectrum region of each star in the NG image referring the 2MASS coordinates and N3 image, and integrate the signal considering the tilt of spectrum. If the stellar spectra partially overlap with each other, we can separate them by a special program developed by Noble et al. (in this volume). Although our reduction tool should work in both 1'×1' and 10'×10' windows, we first applied it to 1'×1' data. In the following, we will show the results from 1'×1' window.

3.2. Continuum

Figure 2 (a) shows a spectrum of a field star behind the molecular cloud L1221. The dots at J, H, K band, 3.6 μm and 4.5 μm depict the photometry data of

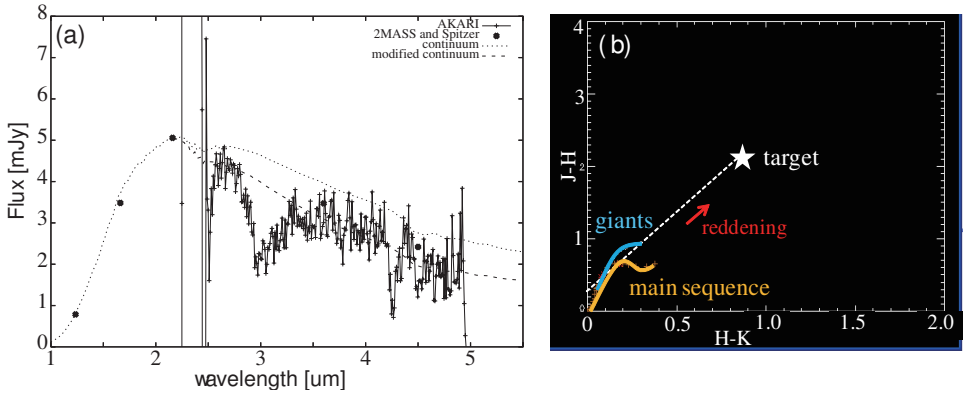

Figure 2. (a) Reduced spectrum of a field star behind L1221 (Solid line). Dotted line is a reddened template spectrum. Dashed line is the continuum which is used to evaluate the ice absorption. (b) Color-color diagram, which is used to estimate the intrinsic stellar spectrum and visual extinction.

2MASS catalog (J, H, and K band) and *Spitzer* archive (3.6μm and 4.5 μm). *AKARI* spectrum agrees well with these photometry values. Water band at 3.05 μm, CO_2 band at 4.27 μm and CO band at 4.67μm are clearly detected.

In order to evaluate the absorption band quantitatively, we need to subtract continuum. We determine the continuum of a field star by estimating the intrinsic spectrum and extinction using color-color diagram (Figure 2 (b)). Horizontal axis is H-K, and vertical axis is J-H. Without extinction, main-sequence stars and giants are plotted on the curves in the left bottom region. If they are reddened by extinction, the (H-K, J-H) points move along the reddening vector. We obtain the J, H, and K magnitude of our target stars from 2MASS catalog, and estimate the intrinsic spectrum by following the reddening vector backwards. The magnitude of the extinction is proportional to the distance between the object and intrinsic spectrum in the diagram. We adopt Weingartner & Draine (2001) as the extinction law, and NextGen model (Hauschildt et al. 1999a,b) as template stellar spectra.

The star shown in Figure 2 (a) is estimated to be a G4 giant with $A_{\rm v}$ = 14.85 mag. The dotted line in Figure 2 (a) is the reddened template spectrum. Agreement of the continuum with the spectrum is good, considering that we use only JHK magnitudes to derive the continuum. But the dotted line seems slightly higher than the spectrum at 3μm and longer. This is probably due to the uncertainties of the extinction law beyond 3 μm. Therefore we modified the extinction law at longer wavelength than K band using polynomial to produce the dashed line in Figure 2 (a), which is used as a continuum to evaluate ice absorption.

In the case of YSOs, we cannot use the color-color diagram to derive the continuum, because their intrinsic colors are not well known. Thus we chose wavelength regions without ice absorption features, and fitted the spectrum with a polynomial.

3.3. Template Ice Spectra

Template ice spectrum have been measured in the laboratories. Gerakines et al. (1995, 1996) measured absorption profiles and determined band strength of various astrophysical ice analogs. Ehrenfreund et al. (1997) pointed out that the band profile depends sensitively on the grain shape, and calculated the profile for several model grains. We obtained these template spectrum from "data base 2007" at Raymond & Beverly Sackler Laboratory for Astrophysics http://www.strw.leidenuniv.nl/~lab/, and convolved them with the point spread function (PSF) of *AKARI*. While 3.05μm band of water is little affected by either the convolution or the grain shape effect, 4.27 μm CO_2 band and 4.67 μm CO band are strongly sensitive to the grain shape, and also are significantly broadened by the PSF. We adopted CDE (continuously distributed ellipsoids) grain model for CO band feature, referring to Pontoppidann et al. (2003). As for CO_2 band, on the other hand, we adopt the spectrum of Gerakines et al. (1995), since it best agrees with the interstellar ice profile observed by ISO (Gerakines et al. 1999).

3.4. Absorption Features and Ice Column Densities

Figure 3 shows the spectrum of a field star behind L1221 normalized by the continuum. We compare the observed absorption feature with the template ice spectra convolved with the PSF. The optical depth of the observed absorption feature is determined by the least-square fitting of the normalized flux with the convolved ice spectra. It should be noted that we use the normalized flux instead of optical depth for the least square fitting, because our CO and CO_2 features are broadened by the PSF and because 3.05 μm water band of some target stars are saturated.

Once we get the best fit absorption spectrum, we go back to the ice spectrum before convolution, and take the logarithm of the spectrum to convert the vertical axis to the optical depth. The column density N of ice is obtained by

$$N = \int \frac{\tau d\nu}{A}, \tag{1}$$

where A is the band strength (e.g. Wittet 1993). We adopt the equation (3) of Pontoppidann et al. (2003) to derive CO ice column densities, since we assume CDE grain model for CO ice.

4. Results

4.1. Field Stars

Figure 4 shows the derived optical depth of H_2O ice and CO_2 ice column densities as a function of estimated visual extinction towards field stars behind molecular clouds. Labels depict the names of the clouds. The optical depth of water is over-plotted on the results of Murakawa et al. (2000) (open circles in Figure 4(a)), who observed 3.05μm water band towards Heiles Cloud 2 using ground-based telescopes. The column density of water ice towards our targets range from 9.7×10^{17} cm^{-2} to 2.0×10^{18} cm^{-2}. CO_2 column density is over-plotted

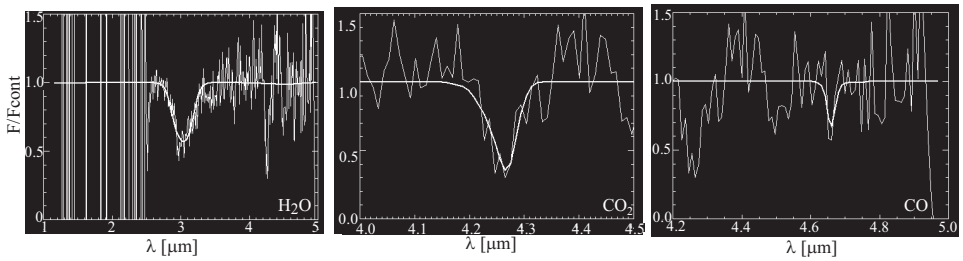

Figure 3. Spectra of a field star behind LDN1221 normalized by the continuum. Absorption bands of H_2O, CO_2 and CO are fitted by a template ice spectrum.

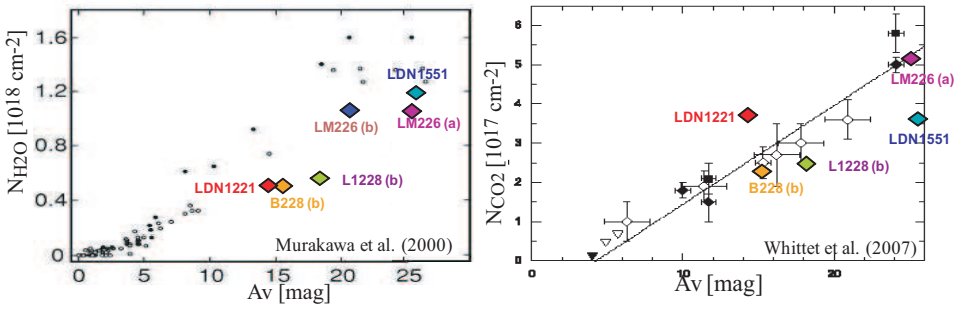

Figure 4. Optical depth of H_2O ice and column density of CO_2 ice as a function of estimated visual extinction towards field stars behind molecular clouds. Results of *AKARI* observation is over-plotted on the water ice observation by Murakawa et al. (2000) and *Spitzer* observation of CO_2 by Whittet et al. (2007). Reproduced by permission of the AAS.

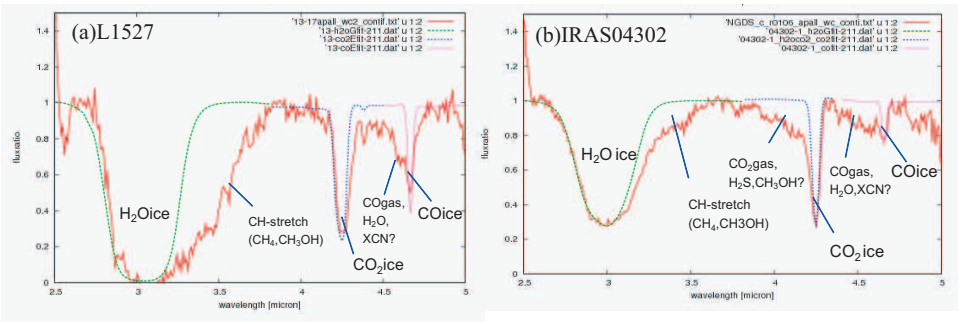

Figure 5. *AKARI* spectrum of YSOs with edge-on disks (a) L1527 and (b) IRAS04302+2247. Dotted lines depict the best-fit of the template ice spectrum.

on the results of Whittet et al. (2007), who observed field stars behind Taurus molecular clouds using *SST* (open squares in Figure 4(b)).

While the optical depth of water ice shows good correlation with $A_{\rm v}$, correlation of CO_2 with $A_{\rm v}$ is worse than that of water. It could be caused by low S/N at 4 μm. At the absorption peak of CO_2 band, the measured flux is $\sim 1\mu$m, which is almost the noise level of our observation. Correlation of CO ice column density with $A_{\rm v}$ (which is now shown here) is still worse than that of CO_2.

4.2. YSO

Figure 5 shows the spectrum of L1527 and IRAS04302+2247, which are class 0 objects with edge-on disks. They are normalized by a continuum, which is the polynomial fit to the spectrum. We see additional absorption features to the H_2O, CO_2 and CO bands. The absorption at $\sim 3.5\mu$m indicates the C-H stretch of CH_3OH and/or aliphatic species. Short wavelength wing of the CO_2 band in IRAS04302 can either be CO_2 gas, H_2S ice, or CH_3OH ice. Absorption at $\sim 4.5\mu$m in both sources can be either CO gas, H_2O ice or XCN.

The derived ice column densities are listed in Table 1. If the water band is saturated, we estimated the water ice column density by fitting the short wavelength wing of the band (Figure 5). L1527, L1041 and IRAS04302 are class 0-I. We detected ice material either in the disk or envelope, or both. ASR41, on the other hand, is classified as class II. The water ice detected towards ASR41 can thus originate in the disk. Both HK Tau and HV Tau are binary system; in both systems, the class II object with edge-on disk is a secondary object fainter than the primary star. So far, we have not disentangles the binary spectra, and the spectrum is dominated by the primary. We may be seeing ice in the foreground clouds.

5. Summary

We observed ice absorption bands at NIR (2.5μm-5.0μm) towards field stars behind molecular clouds and low-mass YSOs with edge-on disk. Absorption bands of H_2O, CO_2 and CO are clearly detected. The column density of H_2O ice towards our target stars range from 3×10^{17}cm^{-2} to 1×10^{19} cm^{-2}, while CO_2

Table 1. Ice column densities towards YSOs

Object	class	N(H_2O) 10^{17} cm^{-2}	N(CO_2) 10^{17} cm^{-2}	N(CO) 10^{17} cm^{-2}
L1527	0-I	97.90	6.62	14.19
L1041	0-I	131.44	5.67	15.81
IRAS04302+2247	I	22.06	3.28	3.73
ASR41	II	6.85	-	-
HK Tau	II	3.04	0.92	-
HV Tau	II	5.32	1.10	-

ice column density is $(1-7)\times10^{17}$ cm^{-2}. The spectra towards YSOs contain many other features, which can be CH_3OH ice, XCN ice and gaseous CO and CO_2.

Acknowledgments. This research is based on observations with AKARI, a JAXA project with the participation of ESA. This work was supported by a Grant-in-Aid for Scientific Research (19740103) and by Global COE program "Foundation of the international education and research center for planetary science" of the Ministry of Education, Culture, Sports, Science and Technology of Japan (MEXT).

References

Aikawa, Y., Herbst, E., Roberts, H., & Caselli, P. 2005, ApJ, 620, 330
Ehrenfreund, P., Boogert, A.C.A., Gerakines, P.A., Tielens, A.G.G.M., van Dishoeck, E.F. 1997, A&A 328, 649
Gerakines, P.A., Schutte, W.A., Greenberg, J.M., van Dishoeck, E.F. 1995, A&A. 296, 810
Gerakines, P.A., Schutte, W.A., Ehrenfreund, P. 1996, A&A, 312, 289
Gerakines, P.A. et al.(1999), ApJ, 522, 357
Gibb, E.L., Whittet, D.C.B., Boogert, A.C.A. & Tielens, A.G.G.M. 2004, ApJS, 151, 35
Hauschildt, P.H., Allard, F., Baron, E. 1999, ApJ, 512, 377
Hauschildt, P.H., Allard, F., Ferguson, J., Baron, E., Alexander, D.R. 1999, ApJ, 525, 871
Murakawa, K., Tamura, M. & Nagata, T. 2000, ApJS, 128, 603
Öberg, K. et al. 2008, ApJ, 678, 1032
Pontoppidan, K.M. et al. 2003, A&A, 408, 981
Pontoppidan, K.M. 2006, A&A 453, L47
Pontoppidan, K.M. et al. 2008, ApJ, 678, 1005
Sakon, I.. et al. 2009, ApJ, 692, 546
Stantcheva, T., Shematovich, V. I.., & Herbst, E. 2002, A&A, 391, 1069
Watanabe, N., & Kouchi, A. 2002a, ApJ, 571, L173,
Weingartner, J.C. & Draine, B.T. 2001, ApJ, 548, 296
Whittet, D.C.B. in Dust and Chemistry in Astronomy, ed. T. J. Millar & D. A. Williams(London: Instit. Phys. Publ.), p.9
Whittet, D,C,B., et al. 2007, ApJ, 655, 332